The reactions of pyridinyl thioesters with triiron dodecacarbonyl: Their novel diiron carbonyl complexes and mechanistic investigations

ARTICLE *in* DALTON TRANSACTIONS · JULY 2012

Impact Factor: 4.2 · DOI: 10.1039/c2dt30798g · Source: PubMed

6 AUTHORS, INCLUDING:

Xiaoming Liu
Jiaxing University
90 PUBLICATIONS **2,184** CITATIONS
SEE PROFILE

Zhiyin Xiao
Jiaxing University
28 PUBLICATIONS **95** CITATIONS
SEE PROFILE

Giuseppe Zampella
Università degli Studi di Milano-Bicocca
70 PUBLICATIONS **2,006** CITATIONS
SEE PROFILE

Luca De Gioia
Università degli Studi di Milano-Bicocca
213 PUBLICATIONS **5,283** CITATIONS
SEE PROFILE

Dalton Transactions

Dynamic Article Links

Cite this: *Dalton Trans.*, 2012, **41**, 9482

www.rsc.org/dalton

PAPER

The reactions of pyridinyl thioesters with triiron dodecacarbonyl: their novel diiron carbonyl complexes and mechanistic investigations†

Li Long,[a,b] Zhiyin Xiao,[b] Giuseppe Zampella,*[c] Zhenhong Wei,[a] Luca De Gioia[c] and Xiaoming Liu*[a,b]

Received 13th April 2012, Accepted 22nd May 2012
DOI: 10.1039/c2dt30798g

Reaction of $Fe_3(CO)_{12}$ with pyridinyl thioester ligand $PyCH_2SCOCH_3$ (**L_1**, Py = pyridin-2-yl) produced complex, $[Fe_2(\kappa\text{-}COCH_3)(\mu\text{-}SCH_2Py)(CO)_5]$ (**1**) ($PyCH_2S$ = pyridin-2-ylmethanethiolate). When complex **1** reacted with PPh_3, a monosubstituted complex, $[Fe_2(\kappa\text{-}COCH_3)(\mu\text{-}SCH_2Py)(CO)_4PPh_3]$ (**2**), was derived. Reaction of the same precursor with analogous thioester ligand $PyCH_2SCOPy$ (**L_2**) generated three novel diiron complexes, $[Fe_2(\kappa\text{-}Py)(\mu\text{-}SCH_2Py)(CO)_5]$ (**3**), $[Fe_2(\kappa\text{-}Py)'(\mu\text{-}SCH_2Py)(CO)_5]$ (**4**), and $[Fe_2(\kappa\text{-}Py)(\mu\text{-}SCH_2Py)(CO)_6]$ (**5**). Complexes **3** and **4** are structural isomers. Complex **5** could be converted into complex **4** but the conversion from complex **5** to the isomer **3** was not observed. All the five complexes were fully characterised using FTIR, NMR, and other techniques. Their structures were determined using X-ray single crystal diffraction analysis. The oxidative formation of complexes **1**, **3**, **4**, and **5** involved C–S and/or C–C bonds cleavages. To probe possible mechanisms for these cleavages, DFT calculations were performed. From the calculations, viable reaction pathways leading to the formation of all the isolated products were delineated. The results of the theoretic calculations also allowed rationalisation of the experimental observations.

Introduction

There are three hydrogenases in nature.[1,2] All the three metalloenzymes, [FeFe]-, [NiFe]-, and [Fe]-hydrogenases, possess Fe(I or II)–S and Fe(I or II)–CO bonding features, as shown in Fig. 1.[3–5] Due to the relevance of these enzymes to both catalytic hydrogen production and activation, iron–sulphur–carbonyl chemistry has attracted much attention in recent years. [Fe]-hydrogenase is unlike the other two enzymes in that this enzyme performs its catalysis *via* a specific substrate, methenyltetrahydromethanopterin.[6,7] Structural analysis revealed that the iron centre of the co-factor of the enzyme adopts essentially an octahedral geometry coordinated with a cysteine sulfur atom, two *cis*-CO ligands, a bidentate pyridone derivative which offers two ligating atoms, a pyridone nitrogen and an acyl carbon, and an unidentified ligand which is either mono or diatomic .[3,8–12] Spectroscopic investigations into the cofactor and its mimicking

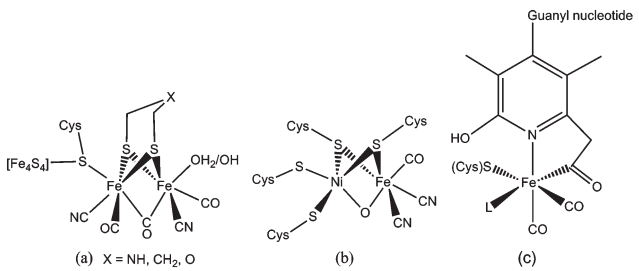

Fig. 1 Schematic views of the metal centres, (a) [FeFe]-, (b) [NiFe]-, and (c) [Fe]-hydrogenases.

chemistry have confirmed that the metal centre is a low spin Fe(II).[13–17]

Modelling the iron centre based on the structural information of the enzyme may not only provide insight into the co-factor, for instance shedding light on the nature of the unknown ligand around the metal centre, but also has relevance to the activation of dihydrogen. In the past few years, attention has been paid on the monoiron centre of this enzyme. Those reported mimics provided insight into the oxidation state of the iron centre and showed the pyridinyl N–Fe(II) and acyl C–Fe(II) bonding feature found in the cofactor.[18–28] It was reported that the reaction of the thioester with either $Fe_3(CO)_{12}$ or $Fe_2(CO)_9$ produced diiron hexacarbonyl complexes with the binding feature of acyl C–Fe(I) bond.[29,30] Recently, Rauchfuss and co-workers reported a type of reaction between thioester ligands and $Fe_2(CO)_9$.[19,22] The oxidative reactions produced "unstable" monoiron complexes bearing the acyl-binding feature which dimerised slowly in solution. Being inspired by this chemistry, we were interested in the reactions of multidentate

[a]*Department of Chemistry, Nanchang University, Nanchang 330031, China*
[b]*College of Biological, Chemical Sciences and Engineering, Jiaxing University, Jiaxing 314001, China. E-mail: xiaoming.liu@mail.zjxu.edu.cn, xiaoming.liu@ncu.edu.cn; Tel: +86 (0)57383643937*
[c]*Department of Biotechnology and Biosciences, University of Milano-Bicocca, 20126 Milano, Italy. E-mail: giuseppe.zampella@unimib.it; Fax: +39 (0)264483478; Tel: +39 (0)264483416*

†Electronic supplementary information (ESI) available: Spectral data of complex **4** and the conversion from complexes **5** to **4** and schematic details and extended descriptions of the reaction pathways generated from DFT calculations. CCDC 860436–860440 for complexes **1**–**5**. For ESI and crystallographic data in CIF or other electronic format see DOI: 10.1039/c2dt30798g

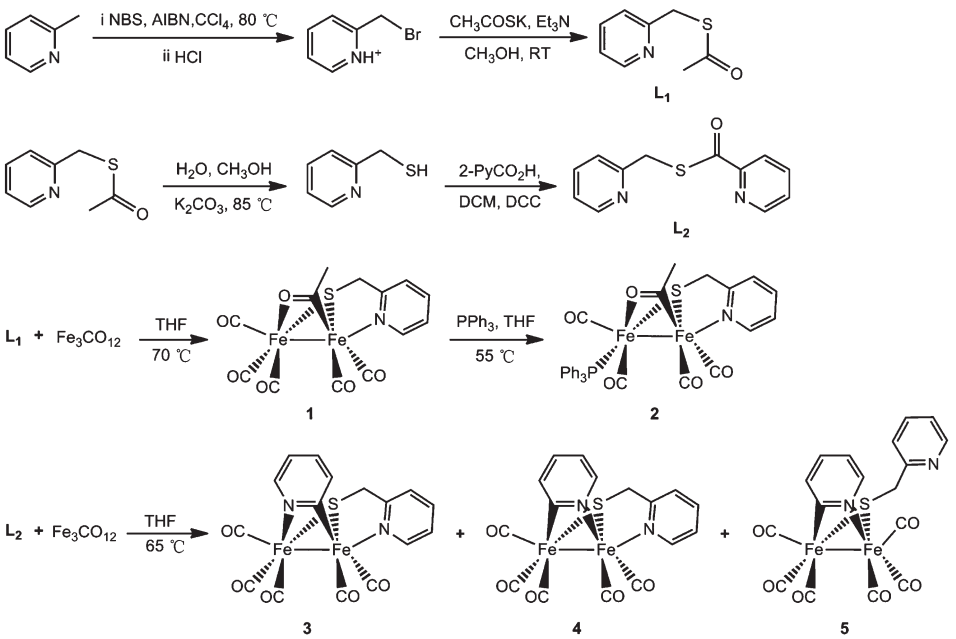

Scheme 1 Synthetic route of ligands $\mathbf{L_1}$, $\mathbf{L_2}$, and complexes **1–5** (DCM = dichloromethane, DCC = dicyclohexylcarbodiimide).

ligands bearing both pyridinyl and thioester moieties with $Fe_3(CO)_{12}$. This is because not only has the triiron carbonyl cluster been a precursor widely employed in the preparation of diiron carbonyl complexes as models of the diiron subunit of the [FeFe]-hydrogenase, but also its reaction often initiates cleavage/formation C–S(N) bonds which may lead to novel complexes/clusters.[29,31]

Herein, we report the synthesis of two thioester ligands, $PyCH_2SCOCH_3$ ($\mathbf{L_1}$) and $PyCH_2SCOPy$ ($\mathbf{L_2}$), their reactions with $Fe_3(CO)_{12}$ and derived novel diiron complexes (please note that throughout this work, Py denotes the pyridin-2-yl group). Mechanistic investigations into the reactions were also performed using DFT calculations. Both ligands gave novel diiron complexes involving the cleavages of C–S and C–C bonds of the ligands. For ligand $\mathbf{L_1}$, complex $[Fe_2(\kappa\text{-}COCH_3)(\mu\text{-}SCH_2Py)(CO)_5]$ (**1**) was isolated. Further reaction of complex **1** with PPh_3 afforded substituted complex $[Fe_2(\kappa\text{-}COCH_3)(\mu\text{-}SCH_2Py)(CO)_4PPh_3]$ (**2**) without affecting the diiron integrity. While in the reaction of ligand $\mathbf{L_2}$, three complexes, $[Fe_2(\kappa\text{-}Py)(\mu\text{-}SCH_2Py)(CO)_5]$ (**3**), $[Fe_2(\kappa\text{-}Py)'(\mu\text{-}SCH_2Py)(CO)_5]$ (**4**) and $[Fe_2(\kappa\text{-}Py)(\mu\text{-}SCH_2Py)(CO)_6]$ (**5**), were produced, of which complexes **3** and **4** are structural isomers with subtle differences in the coordination of the pyridin-2-yl group to the diiron centre. Under the aid of decarboxylating agent (Me_3NO), complex **5** was irreversibly converted into complex **4** but no complex **3** was observed. All the complexes were fully characterised using FTIR, $^1H/^{13}C$ NMR, X-ray crystallography. Plausible reaction pathways leading to those diiron complexes were also delineated using DFT calculations.

Results and discussion

Synthesis of thioester ligands ($\mathbf{L_1}$ and $\mathbf{L_2}$) and their reactions with $Fe_3(CO)_{12}$

Ligand $\mathbf{L_1}$ was prepared from 2-methylpyridine through bromination[32,33] and then thioesterisation with thioacetate.[34] The other ligand ($\mathbf{L_2}$) was further derived *via* two-step synthesis, Scheme 1. In the preparation of ligand $\mathbf{L_2}$, the conversion of ligand $\mathbf{L_1}$ into pyridin-2-ylmethanethiol *via* hydrolysis[35,36] was nearly quantitative and its reaction with picolinic acid with the aid of DCC (dicyclohexylcarbodiimide) to achieve ligand $\mathbf{L_2}$ was also in satisfactory yield (*ca*. 90%). The stretching frequency of the carbonyl group of ligand $\mathbf{L_2}$ is 20 cm^{-1} higher than that of ligand $\mathbf{L_1}$ due to the deficiency in electrons of the adjacent pyridin-2-yl group.

Reaction of $Fe_3(CO)_{12}$ with ligand $\mathbf{L_1}$ in THF afforded a diiron pentacarbonyl complex as the sole isolatable product with an $\{Fe^IFe^I\}$ core, $[Fe_2(\kappa\text{-}COCH_3)(\mu\text{-}SCH_2Py)(CO)_5]$ (**1**), Scheme 1. Unlike other analogues widely reported,[37–41] one of the bridging linkages is an acetyl group in a κ-coordinating mode. Such a coordinating mode for acetyl group in a diiron analogue could also be achieved by nucleophilic attack on a bound carbon monoxide by a methyl anion, such as $LiCH_3$, or electrophilic reaction of methyl iodide or acetyl chloride with metal carbonyl anion,[42,43] in addition to the methodology described by Seyferth and co-workers.[29,30] Due to its asymmetric bridging linkages which degrade the entire symmetry of this molecule, complex **1** shows slightly more complicated infrared spectral profile (Fig. 2) compared to other diiron analogues.[38–41] The major difference lies in the middle of the spectrum, as shown in Fig. 2. In complex **1**, it is a main band with a well-resolved shoulder at its right side rather than a single band as observed in the analogues reported previously.[38–41]

Since ligand $\mathbf{L_2}$ is rather similar to ligand $\mathbf{L_1}$ (Scheme 1), one could expect that its reaction with the same triiron precursor would exhibit rather similar chemistry. But, in fact, the reaction for this ligand showed significant differences in that (i) both hexacarbonyl (**5**) and pentacarbonyl (**3** and **4**) products were isolated and, particularly, the pentacarbonyl products were structural isomers (**3** and **4**), and (ii) the bridging linkage is not a picolinoyl group analogous to the acetyl moiety as found in complex

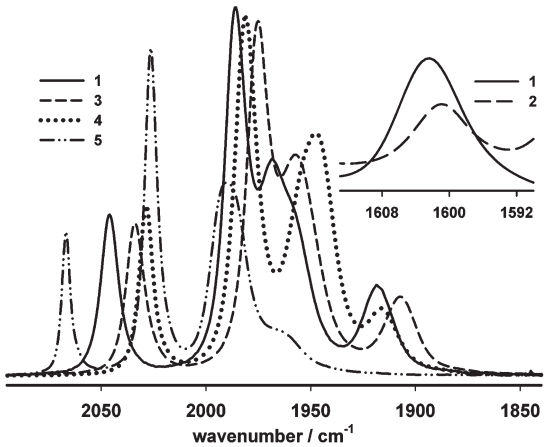

Fig. 2 Infrared spectra of complexes **1**, **3**, **4**, and **5** in dichloromethane. Inset: stretching bands for the bound bridging acetyl group in complexes **1** and **2** (KBr pellets).

1, generated from the cleavage of S–CO(pyridin-2-yl) bond. Instead, it is a pyridin-2-yl group, the decarboxylated species of picolinoyl group. The pyridin-2-yl group bridged the two iron atoms in a κ-coordinating mode in two manners to give the two structural isomers (**3** and **4**), Scheme 1. Due to the same cause as for complex **1**, the three complexes isolated from the reaction of ligand $\mathbf{L_2}$ with $Fe_3(CO)_{12}$ show also more absorption bands compared to their analogues with symmetric bridging linkages.[38,39,41,44,45] It is not uncommon that in both Ru and Os dinuclear complexes, a pyridin-2-yl anion binds isomerically.[46,47] But this isomeric binding has not been observed for a diiron complex although one of the analogous structures was recently reported.[48] The two isomers have very similar absorption bands in their FTIR spectra, as shown in Fig. 1. In their proton magnetic resonance, only subtle differences in the chemical shifts of the pyridin-2-yl rings in complexes **3** and **4** were observed. It is noteworthy that complex **5** could be cleanly converted into complex **4** under the aid of a decarboxylating agent, as indicated spectroscopically (Fig. S1†). This conversion is informative in deducing the reaction mechanism of the ligands with the triiron precursor. Indeed, theoretic calculations revealed that it is a viable pathway (*vide infra*). But, interestingly, an analogous conversion into complex **3** was not observed. This observation is particularly peculiar as both sterically and electronically the two $\{Fe(CO)_3\}$ units are generally identical and classic *cis*-/*trans*-effect would not be sufficient to explain this discrimination in the intramolecular substitution reaction.

Reaction of PPh_3 with complex **1** produced a mono-substituted diiron pentacarbonyl complex as with other reported diiron analogues,[49] $[Fe_2(\kappa\text{-}COCH_3)(\mu\text{-}SCH_2Py)(CO)_4PPh_3]$ (**2**), with both the acetyl binding and Fe–Fe bond intact, Scheme 1. The resultant product exhibits generally similar infrared spectral pattern to those diiron tetracarbonyl analogues reported but again the asymmetric bridging linkages increase the multiplicity of its infrared spectrum in the absorption region of CO (Fig. S2†).[40] In solution, both complexes do not show any absorption band for the bridging acetyl group but in the solid state a weak band is evident around 1600 cm^{-1}, Fig. 2 (inset).

Structural analysis

The five diiron carbonyl complexes are all reasonably stable in solution. Diffusion of hexanes into solutions of these complexes in dichloromethane afforded deep-coloured crystals of complexes **1–5**. The crystals were suitable for X-ray single crystal diffraction analysis. Crystallographic details of these complexes are tabulated in Table 1. Their structural views are shown in Fig. 3–5. Like other diiron carbonyl complexes reported in the literature,[37–41,44,45] the iron atoms adopt essentially slightly distorted octahedral geometries, as shown by the selected bonding parameters for the five complexes summarised in Table 2. For complexes **1–4**, it is noticeable that the bond length of the Fe1–S bond is shorter by 0.3 to 0.5 Å compared to the Fe2–S1 bond. This shortening is mainly caused by the binding of the pyridinyl N. The Fe1–N1 and Fe1–S1 bonds are parts of a 5-membered ring which is nearly an isosceles pentagon. In complexes **1** and **2**, the κ-bridging acetyl bond has a length of 1.26 Å, about 0.1 Å longer than the end-on binding acyl group,[20] which is probably attributed to both its κ-bridging nature and lower oxidation state in the two complexes. Distinguishing crystallographically the binding modes offered by the C and N atoms of the pyridin-2-yl anion to the diiron centre in the structural isomers **3** and **4** is a nontrivial task since the two neighbouring atoms are electronically highly similar. Repetitively preparing single crystals with high quality allowed us to determine unequivocally the proper assignment of the two structural isomers. It is interesting to note that the Fe1–C13 bond in complex **3** is shorter by 0.03 Å than the Fe2–C13 bond in complex **4**, and similar shortening for the two Fe1–N2 bonds in complexes **3** and **4** is also observed. In other words, the bond Fe–X (X = Cl3 and N2) *trans* to CO is always longer than its analogous bond *trans* to pyridinyl group on the other iron atom. This is likely attributed to the difference in *trans* effect exerted by CO and the pyridinyl group, respectively.

Possible pathways for the cleavage of C–S (complexes 1, 3, 4, and 5) and C–C(Py) bonds (complexes 3, 4, and 5)

Oxidative reaction of triiron dodecacarbonyl, $Fe_3(CO)_{12}$, with thiols could involve cleavage/formation of C–C and/or C–X (X = S, N) bonds to produce unexpected diiron complexes depending on the nature of the thiols employed.[29–31] In the reaction of $Fe_2(CO)_9$ with thioesters,[19,22] the formation of diiron complexes involving acyl binding were achieved *via* unstable monoiron intermediate. Therefore, it is feasible to speculate that the reaction of $Fe_3(CO)_{12}$ with ligands $\mathbf{L_1}$ and $\mathbf{L_2}$ would adopt a similar pathway. Upon the reaction of the ligands with the triiron precursor, a key monoiron intermediate *via* the cleavage of the C–S bond of the thioester ligands could form, Scheme 2. It is noteworthy that, in the case of ligand $\mathbf{L_2}$, the picolinoyl is further decarboxylated to generate a pyridin-2-yl group after the C–S bond cleavage. Possibly, the initially formed picolinoyl is unstable, probably due to the electron-deficient nature of the pyridinyl group. Further reaction of the monoiron intermediate with iron–carbonyl, either the precursor or the fragments generated in the reaction, $\{Fe(CO)_n\}_m$ (m = 1–3, $n > 0$), produced complexes **1**, **3**, **4**, and **5**, Scheme 2. More details about the cleavage mechanism and reaction pathways were obtained by theoretic investigations.

Table 1 Crystallographic data and processing parameters for complex **1–5**[a]

Complex	**1**	**2**	**3**	**4**	**5**
Formula	$C_{13}H_9Fe_2NO_6S$	$C_{30}H_{24}Fe_2NO_5PS$	$C_{16}H_{10}Fe_2N_2O_5S$	$C_{16}H_{10}Fe_2N_2O_5S$	$C_{17}H_{10}Fe_2N_2O_6S$
M_w (g mol^{-1})	418.98	653.24	454.03	454.03	482.04
T (K)	296(2)	296(2)	296(2)	296(2)	296(2)
Crystal system	Triclinic	Triclinic	Monoclinic	Triclinic	Orthorhombic
Space group	$P\bar{1}$	$P\bar{1}$	$P21/c$	$P\bar{1}$	$Pccn$
a (Å)	8.034(2)	9.0878(18)	8.784(5)	9.0510(19)	16.518(2)
b (Å)	8.357(2)	12.580(3)	12.502(7)	9.2243(19)	18.976(3)
c (Å)	12.834(4)	13.299(3)	16.016(8)	11.929(4)	12.3490(17)
α (°)	98.666(3)	69.848(2)	90	101.145(3)	90.00
β (°)	93.134(3)	84.859(2)	92.832(6)	102.516(3)	90.00
γ (°)	110.001(3)	88.663(2)	90	107.424(2)	90.00
V [Å^3]	795.2(4)	1421.5(5)	1756.6(16)	891.3(4)	3870.74
Z	2	2	4	2	8
D_{calcd} (g cm^{-3})	1.750	1.526	1.717	1.692	1.654
F (000)	420.0	668.0	912.0	456.0	1936.0
θ (°)	2.64–28.37	2.25–28.47	2.32–28.35	2.41–28.31	2.32–28.30
Reflns collected/ unique	7478/3987	13 543/7181	15 226/4391	8239/4293	34 515/4818
GOF on F^2	1.034	1.008	1.030	0.999	1.040
R_1 [$I > 2\sigma(I)$]	0.0221	0.0299	0.0654	0.0242	0.0472
wR_2 [$I > 2\sigma(I)$]	0.0594	0.0821	0.1545	0.0638	0.1224
Residual electron density (e Å^{-3})	0.298, −0.320	0.348, −0.495	1.402, −0.813	0.346, −0.312	1.538, −0.614

[a] $R_1 = \sum||F_o| - |F_c||/\sum|F_o|$ and $wR_2 = [\sum(|F_o^2 - F_c^2|)^2/\sum(wF_o^2)^2]^{\frac{1}{2}}$.

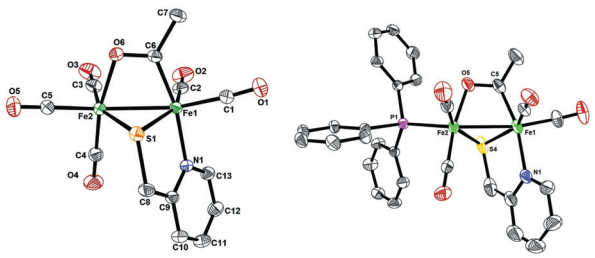

Fig. 3 Crystal structures of complexes **1** (left) and **2** (right) (ellipsoids were drawn at probability level of 30% and hydrogen atoms were omitted for clarity).

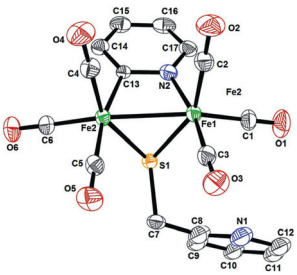

Fig. 5 Crystal structure of complex **5** (ellipsoids were drawn at probability level of 30% and hydrogen atoms were omitted for clarity).

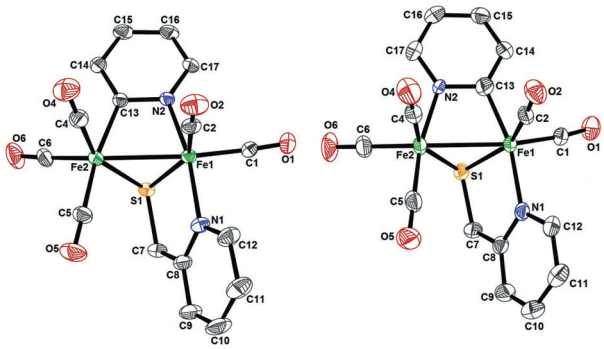

Fig. 4 Crystal structures of complexes **3** (left) and **4** (right) (ellipsoids were drawn at probability level of 30% and hydrogen atoms were omitted for clarity).

DFT calculations

As mentioned above, it is difficult to sketch out more detailed reaction pathways than those shown in Scheme 2 due to the complexity of the reactions and impossibility in isolating any stable intermediates. To explore possible relevant pathways to delineate the reaction mechanisms for the formation of the diiron complexes, a series of theoretic calculations were carried out using DFT protocols previously validated in the study of models of the [FeFe]-hydrogenase active site.[50–57]

The results of DFT calculations allowed us to outline the main features of the reaction pathways of both ligands with $Fe_3(CO)_{12}$. Due to the multiplicity of the reaction pathways and the large number of transition states and intermediates involved, we depict the reaction mechanisms in a highly simplified manner in Schemes 3 and 4, respectively, and leave the very detailed schemes in ESI† for further reference. Therein has been also reported an extended description to complement all the Schemes.†

We must point out that the same denotation shown in the two schemes (Schemes 3 and 4) does not necessarily mean exactly the same species. To envision clearly all the pathways shown in the two schemes leading to the complexes (**1**, **3**, **4**, and **5**), those reaction pathways and related energies were also tabulated in Tables 3 and 4, respectively. In such Tables and related Schemes,

Table 2 Selected bond lengths and angles for complex **1–5**

Complex	**1**	**2**	**3**	**4**	**5**
Fe1–Fe2	2.5626(6)	2.5535(6)	2.5932(16)	2.5938(6)	2.5778(7)
Fe1–S1	2.2195(6)	2.2369(6)	2.2080(16)	2.2269(5)	2.2400(10)
Fe2–S1	2.2672(6)	2.2762(7)	2.2673(17)	2.2604(7)	2.2515(10)
Fe1–N1	2.0594(13)	2.0643(19)	2.028(4)	2.0112(13)	
Fe2–N2			1.979(4)		
Fe1–N2 (*trans* to Py)				1.9649(12)	1.981(3)
Fe1–C13 (*trans* to Py)			1.956(4)		
Fe2–C13				1.9839(15)	1.984(3)
C1–O1	1.140(2)	1.141(2)	1.150(6)	1.138(2)	1.130(6)
C6–O6 (Acyl)	1.2555(19)	1.261(2)			

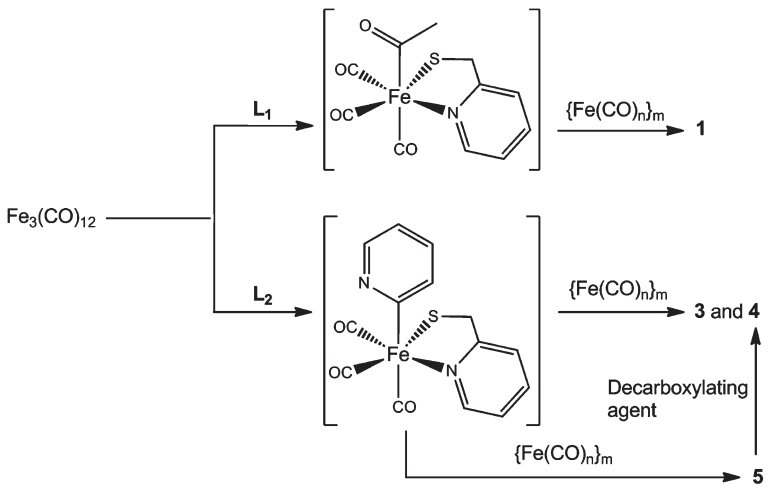

Scheme 2 The formation of complexes **1**, **3**, **4**, and **5** involving hypothesised monoiron intermediates ($\{Fe(CO)_n\}_m$ could be either the triiron precursor or a fragment generated in the reaction).

the denotation $^{D}\mathbf{L}_n$ refers to the ligands ($\mathbf{L_1}$ and $\mathbf{L_2}$) with an appropriate donor atom (**D**) which initiates the reaction with the triiron precursor.

As for the diiron unit formation, a possible route might imply a single-step reaction of the ligands with the triiron precursor by simply ejecting a monoiron–carbonyl fragment. However, DFT results indicate that the diiron core can be assembled following a stepwise reaction pathway. The first iron atom was abstracted when the ligand reacted with the triiron precursor and a $\{Fe_2(CO)_8\}$ fragment was cleaved. This cleavage was highly thermodynamically favoured. Other cleavages have been taken into account such as a single CO releasing from $Fe_3(CO)_{12}$ upon $\mathbf{L_1}$/$\mathbf{L_2}$ addition, but they all resulted in kinetically disfavoured pathways (associated barrier higher by 24 kcal mol^{-1} than those associated to the presented reaction routes). The formed monoiron species underwent further reactions and the second iron was added to the monoiron unit *via* its reaction with the precursor. An attempt has been made to explore catalytic effects of labile species (such as $Fe_2(CO)_8$), which may be possibly present in solution as by-products of the early step of the reaction of the ligands ($\mathbf{L_1}$/$\mathbf{L_2}$) with $Fe_3(CO)_{12}$. Even though it is conceivable that such unsaturated species may react with CO molecules which are released during some of the steps along the investigated pathway, it is interesting to explore the extent of decrease on the activation barrier of key steps, such as the iron unit incorporation, which can be exerted by possibly existing accelerators (such as $Fe_2(CO)_8$). DFT data indicate that the energy barrier associated to the transfer of the mono-iron unit is actually decreased by evident and different amounts in the different pathways investigated.

It was experimentally observed in the reactions involving both ligands that increasing the ratio of the triiron precursor over the ligand from 1 : 1 to 2 : 1 could almost double the overall reaction yield. This suggests that involvement of the triiron precursor could be dominant in assembling the second iron into the diiron core. The outlined pathways are consistent with this observation. As shown in Tables 3 and 4, the formation of all the products is overall exergonic. The multidentate nature of the ligands offered several ways to initiate the reactions. But no matter which donor atom of the ligands attacked first at one of the three iron atoms of the precursor, the right first step was kinetically up-hill with an associated $\Delta G^{\ddagger}$ of *ca.* 30 kcal mol^{-1}. This explains well that heating was necessary to drive the reactions to proceed. For both ligands, their reactions with the triiron precursor involved bond cleavage of C–S and/or C–C bonds before the final products formed. Such a bond cleavage could occur either before or after the diiron unit was assembled. In either way, those bond cleavages are highly exergonic.

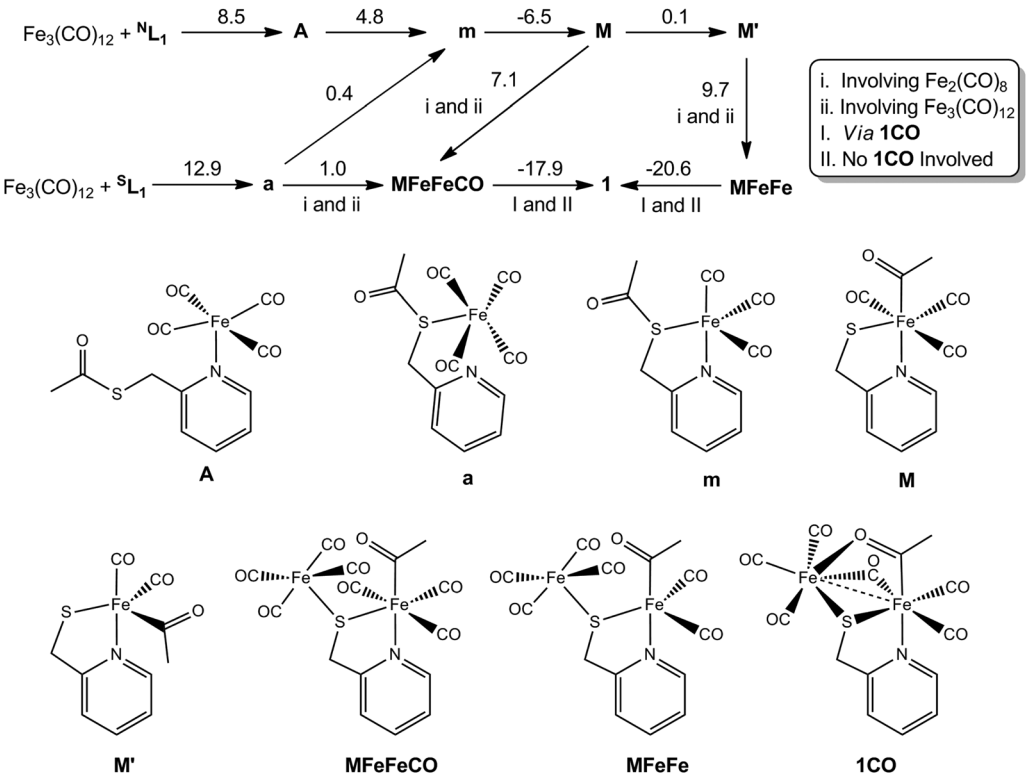

Scheme 3 Reaction pathways leading to the formation of complex **1** as derived from DFT calculations, related energies (kcal mol^{-1}), and the calculated structures of the intermediates involved in the reactions.

The reaction pathways revealed by the theoretic calculations for ligand $\mathbf{L_2}$ showed that the reaction did not lead directly to diiron pentacarbonyl complexes. Instead, the most favourable one among the reaction pathways led to the diiron hexacarbonyl **5**, as shown in Scheme 4a and Table 4. After the reaction between $Fe_3(CO)_{12}$ and $\mathbf{L_2}$ occurred, complexes **5**, **3** and **4** were isolated in an approximate ratio of 2 : 1 : 1, which is in line with the DFT-calculated relative stabilities associated to the three complexes. Although the formation energies for both complexes **3** and **4** are globally exergonic, the energies of the conversion from complexes **5** to **3**/**4** are slightly endergonic (ΔG is 0.5, 1.0 kcal mol^{-1}, respectively; Table 4). This is consistent with the observation that heating a solution of complex **5** did not produce either complexes **3** or **4**. As mentioned earlier, under the aid of decarboxylating agent, complex **5** was solely converted into complex **4** without any of its isomer **3** isolated. This ought to be attributed to kinetic reason of the chemical reaction rather than to thermodynamics matters.

Conclusions

Two pyridinyl thioesters ligands and their reactions with $Fe_3(CO)_{12}$ were described and four novel diiron complexes (**1**, **3**, **4**, and **5**) with κ-$COCH_3$ or -pyridin-2-yl coordination modes were isolated. Reaction of complex **1** with PPh_3 led to complex **2** leaving the κ-$COCH_3$ binding intact. The structural isomers, complexes **3** and **4**, exhibit a subtle difference in the manner of bridging the two iron atoms, κ-(C, N)Py and κ-(N, C)Py. The acetyl ($COCH_3$) or pyridin-2-yl were apparently generated *in situ* in the reactions, that is, resulting from fragmentation of the parent ligands involving C–S and C–C bond cleavage. The chemical features of the obtained complexes were established using FTIR, NMR spectroscopies, and microanalysis. Their crystal structures were also determined using X-ray single crystal diffraction analysis.

DFT calculations provided some insight into the reaction mechanisms of the triiron carbonyl precursor with the ligands, $\mathbf{L_1}$ and $\mathbf{L_2}$, and disclosed multiple plausible pathways leading to the novel diiron products. The S atom has a slight preference over the N atom in the reaction with the triiron precursor according to the theoretical data. The diiron unit of the complexes was assembled stepwise rather than retaining a diiron core by cleaving a monoiron carbonyl fragment in the reaction with the triiron cluster $Fe_3(CO)_{12}$. During the various reaction occurrences, the cleavage of the acetyl groups (acetyl, CH_3CO and picolinoyl, PyCO) occurring *via* breaking the C–S bond is thermodynamically spontaneous. Further cleavage of one CO from the group, 2-PyCO, was also strongly favoured. These bond cleavages were certainly driven by the coordination of different ligands (S, N, O) to the metal atom. Since triiron dodecacarbonyl cluster ($Fe_3(CO)_{12}$) is a universal precursor leading to other iron–carbonyl complexes, understanding mechanistically its reaction would certainly make its products more predictable and, therefore, be beneficial to designing novel diiron–carbonyl complexes, which are widely regarded as mimics of the diiron subunit of the [FeFe]-hydrogenase.

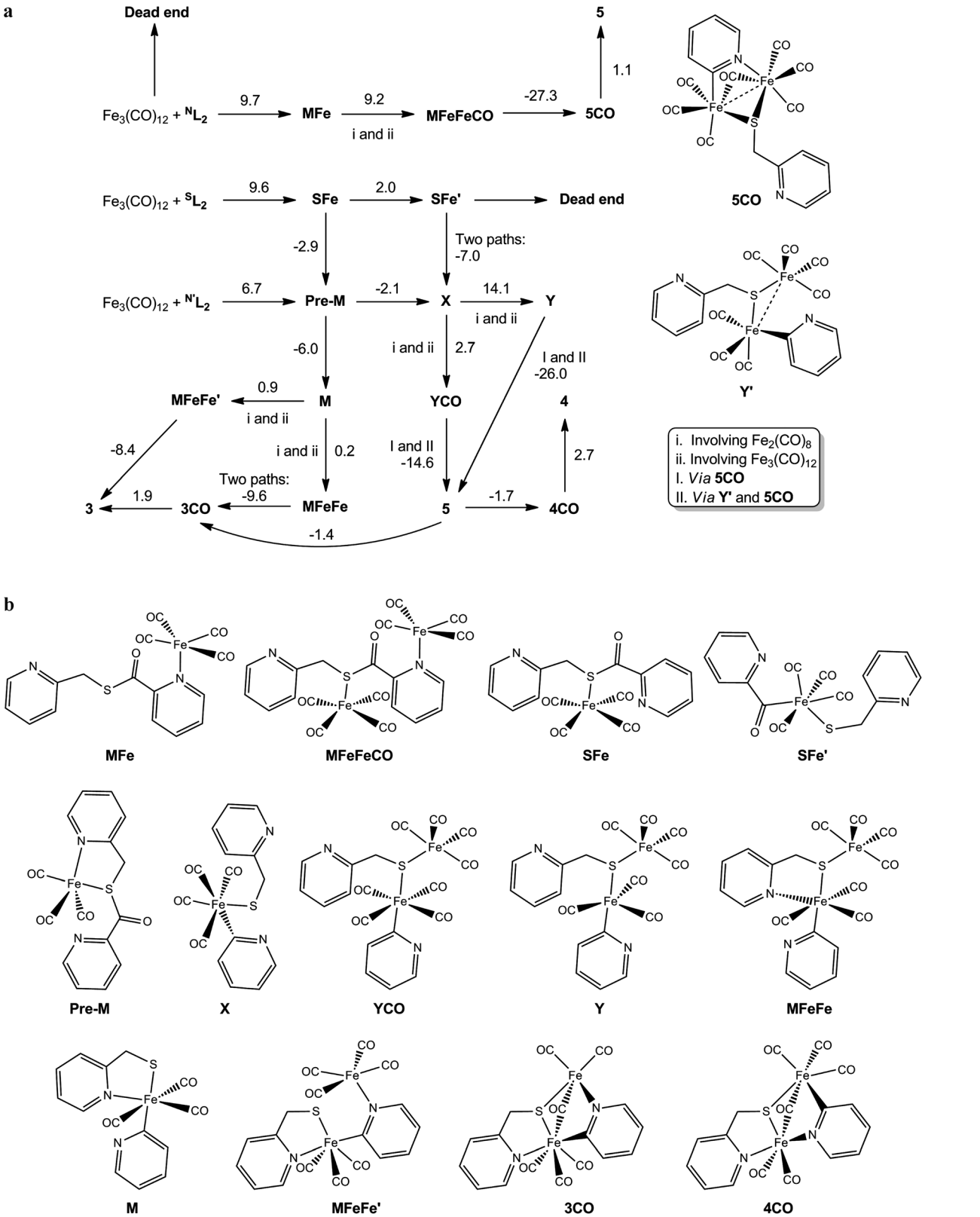

Scheme 4 (a) Reaction pathways leading to the formation of complexes **3**, **4**, and **5** as derived from DFT calculations and related energies (kcal mol^{-1}). Please note that **N′** in $^{N'}L_2$ refers to the N atom of the pyridinyl ring bearing a methylene group and the calculated structures of those intermediates are shown in Scheme 4b except for **5CO** and **Y′**. (b) Key intermediates involved in the reaction pathways shown in Scheme 4a.

Table 3 Reaction pathways ($^1\mathbf{P}_n$) of the triiron precursor with ligand $\mathbf{L_1}$ and related energies (kcal mol^{-1})

$^{D}L_1$ [a]	^1P_n	Reaction pathway	ΔG	$\Delta G'$ [b]
$^{N}L_1$	$^1P_1$	→ A → m → M → M′ → MFeFe → **1**	−4.0	30.2
	$^1P_2$	→ A → m → M → MFeFeCO → **1**	−4.0	
$^{S}L_1$	$^1P_3$	→ a → MFeFeCO → **1**	−4.0	28.3
	$^1P_4$	→ a → m → M → MFeFeCO → **1**	−4.0	
	$^1P_5$	→ a → m → M → M′ → MFeFe → **1**	−4.0	

[a] D refers to donor atoms, N and S. [b] $\Delta G'$ refers to the energy involved in the right first step of the ligand attacking the triiron precursor.

Table 4 Reaction pathways ($^2\mathbf{P}_n$) of the triiron precursor with ligand **L** and related energies (kcal mol^{-1})

$^{D}L_2$ [a]	^2P_n	Reaction pathway	ΔG	$\Delta G'$ [b]
$^{N}L_2$	$^2P_1$	→ MFe → MFeFeCO → 5CO → **5**	−7.3	32.0
	$^2P_2$	$^2P_1$ (**5**) → 3CO → **3**	−6.8	
	$^2P_3$	$^2P_1$ (**5**) → 4CO → **4**	−6.3	
$^{S}L_2$	$^2P_4$	→ SFe → SFe′ → X → Y → **5**	−7.3	31.8
	$^2P_5$	→ SFe → SFe′ → X → YCO → **5**	−7.3	
	$^2P_6$	→ SFe → Pre-M → X → Y → **5**	−7.3	
	$^2P_7$	→ SFe → Pre-M → X → YCO → **5**	−7.3	
	$^2P_8$	→ SFe → Pre-M → MFeFe → 3CO → **3**	−6.8	
	$^2P_9$	→ SFe → Pre-M → MFeFe′ → **3**	−6.8	
	$^2P_{10}$	$^2P_4$ (**5**) → 3CO → **3**	−6.8	
	$^2P_{11}$	$^2P_5$ (**5**) → 3CO → **3**	−6.8	
	$^2P_{12}$	$^2P_6$ (**5**) → 3CO → **3**	−6.8	
	$^2P_{13}$	$^2P_7$ (**5**) → 3CO → **3**	−6.8	
	$^2P_{14}$	$^2P_4$ (**5**) → 4CO → **4**	−6.3	
	$^2P_{15}$	$^2P_5$ (**5**) → 4CO → **4**	−6.3	
	$^2P_{16}$	$^2P_6$ (**5**) → 4CO → **4**	−6.3	
	$^2P_{17}$	$^2P_7$ (**5**) → 4CO → **4**	−6.3	
$^{N'}L_2$	$^2P_{18}$	→ Pre-M → X → Y → **5**	−7.3	34.6
	$^2P_{19}$	→ Pre-M → X → YCO → **5**	−7.3	
	$^2P_{20}$	→ Pre-M → M → MFeFe → 3CO → **3**	−6.8	
	$^2P_{21}$	→ Pre-M → M → MFeFe′ → **3**	−6.8	
	$^2P_{22}$	$^2P_{18}$ → 3CO → **3**	−6.8	
	$^2P_{23}$	$^2P_{19}$ → 3CO → **3**	−6.8	
	$^2P_{24}$	$^2P_{18}$ → 4CO → **4**	−6.3	
	$^2P_{25}$	$^2P_{19}$ → 4CO → **4**	−6.3	
		5 → 4CO → **4**	1.0	
		5 → 3CO → **3**[c]	0.5	

[a] D refers to donor atoms, N, N′, and S (please refer to the caption of Scheme 4a for the nature of N′). [b] $\Delta G'$ refers to the energy involved in the right first step of the ligand attacking the triiron precursor with a specific donor atom (N, N′, and S). [c] This conversion was not experimentally observed.

Experimental

General procedures

Unless otherwise stated, all operations were carried out under Ar atmosphere using standard Schlenk techniques. Reaction vessels were oven-dried at 150 °C prior to use. Solvents were dried prior to use following to standard procedures. $Fe_3(CO)_{12}$ were synthesised following modified literature procedures.[19,58] FTIR spectra were recorded on Scimitar 2000 (Varian) using a cell with a spacer of 0.1 mm or KBr pellets. NMR spectra were measured on Bruker Avance (400 or 600 MHz) with tetramethylsilane as internal standard. Elemental analyses were performed on a Heraeus CHN–O-Rapid.

Crystal structure analyses

In the crystallographic data collection of complexes **1–5**, standard procedures were used for mounting the crystals on a Bruker CCD area detector diffractometer at 296(2) K. Crystals were routinely coated with paraffin oil before being mounted. Intensity data were collected using Mo Kα radiation (λ = 0.71073 Å) by a φ- and ω-scan mode. The SMART and SAINT programs were used for integration and absorption correction. The structures were solved by direct method using SHELXS program and refined on F^2 with SHELXTL.[1] All non-hydrogen atoms were refined anisotropically and all hydrogen atoms were included at calculated positions with fixed thermal parameters.

DFT calculations

Density functional theory (DFT) calculations have been carried out by adopting the TURBOMOLE suite of programs,[59] at the B-P86/TZVP[60,61] level of theory, which has been reported to be suitable for investigating [FeFe]-hydrogenase models.[50–52,54–57] All kinds of stationary points on the potential energy surface have been determined by means of energy gradient techniques and a full vibrational analysis has been carried out to further characterise each point. Transition state structures have been searched by a procedure based on a pseudo-Newton-Raphson algorithm.

Preliminarily, the geometry optimization of a guessed transition state structure is carried out by freezing the molecular degrees of freedom corresponding to the reaction coordinate (RC). After performing the vibrational analysis of the constrained minimum energy structures, the negative eigenmode associated to the RC is followed to locate the true transition state structure, which corresponds to the maximum energy point along the trajectory which joins two adjacent minima.

Free energy (G) values have been obtained from the electronic SCF energy considering three contributions to the total partition function (Q), namely $q_{translational}$, $q_{rotational}$, $q_{vibrational}$, under the approximation that Q may be written as the product of such terms. Evaluation of H and S contributions has been made by setting T and P values at 298.15 K and 1 bar, respectively.

In all steps investigated which entailed the presence of $Fe_2(CO)_8$ and $Fe(CO)_4$, the energy difference existing between the S = 0 state and the S = 1 state has been taken into account at the same level of theory that has been adopted for the present investigation. The B-P86 functional is known to yield a small energy split between the two different spin states, which is slightly less than that found by wave-function based methods, *i.e.* high correlated post-HF methods such as CCSD and CCSD(T).[62–64]

In light of available experimental data and considering the chemical nature of the ligands, only low-spin species of Fe complexes, which have been subjected to DFT analysis, have been considered.

Synthesis

Preparation of $PyCH_2SCOCH_3$ (L_1). 2-Bromomethyl pyridine hydrochloride (1.00 g, 4.8 mmol), triethylamine (1.4 mL, 9.6 mmol) and CH_3COSK (0.55 g, 4.8 mmol) in methanol (20 mL) were stirred for 2 h at room temperature. After being concentrated under vacuum, the solution was extracted with ethyl acetate (6 × 30 mL). The organic phases were combined and dried with anhydrous $MgSO_4$ before the solvent was removed. Purification of the residue was achieved using flash chromatography (column: silica gel; eluent: a mixture of ethyl acetate–petroleum ether (1 : 4)). The purification gave a colourless oily liquid (0.67 g, 83%). IR (DCM, ν/cm^{-1}): 1695 (–CO). ^{1}H NMR (600 MHz, $CDCl_3$): 8.13 (s, 1H, Py-H), 7.20 (d, J = 2.8 Hz, 1 H, Py-H), 6.94 (s, 1H, Py-H), 6.75 (d, J = 3.1 Hz, 1 H, Py-H), 3.87 (d, J = 5.5 Hz, 2 H, $PyCH_2$), 1.93 (t, J = 1.6 Hz, 3 H, $COCH_3$).

Preparation of $PyCH_2SH$. K_2CO_3 (2.50 g, 18.1 mmol) in H_2O (40 mL) was added to a methanol (50 mL) solution of **L_1** (2.00 g, 12.0 mmol). The mixture was heated to 85 °C and stirred for 2.5 h. The methanol was removed under reduced pressure to give a residual which was extracted using dichloromethane (6 × 30 mL). The organic phases were combined and dried with anhydrous $MgSO_4$ before the solvent was removed. The residue was purified using flash chromatography (eluent: with ethyl acetate–petroleum ether = 1 : 4). A colourless oily liquid was obtained (1.4 g, 94%). ^{1}H NMR (600 MHz, $CDCl_3$): 8.53 (s, 1 H, Py-H), 7.656–7.627 (m, 1 H, Py-H), 7.33 (d, J = 7.8 Hz, 1 H, Py-H), 7.162–7.140 (m, 1 H, Py-H), 3.84 (d, J = 7.2 Hz, 2 H, $PyCH_2$), 2.027 (t, J = 7.8 Hz, 1 H, SH).

Preparation of $PyCH_2SCOPy$ (L_2). To a stirred solution of pyridin-2-ylmethanethiol (1.02 g, 8.1 mmol) in CH_2Cl_2 (DCM) (20 mL) was successively added picolinic acid (1.01 g, 8.1 mmol) and dicyclohexylcarbodiimide (DCC) (1.68 g, 8.1 mmol). The solution was stirred for 3 h at ambient temperature and a white suspended solid was formed. The solid was removed by filtration and the filtrate was concentrated under reduced pressure and purified using column chromatography (eluent: ethyl acetate–petroleum ether = 1 : 1). A white solid (1.65 g, 88%) was obtained. ^{1}H NMR (600 MHz, $CDCl_3$): 8.68 (d, J = 4.20 Hz, 1 H, Py-H), 8.55 (d, J = 4.8 Hz, 1 H, Py-H), 7.97 (d, J = 7.8 Hz, 1 H, Py-H), 7.85 (t, J = 7.5 Hz, 1 H, Py-H), 7.63 (t, J = 7.5 Hz, 1 H, Py-H), 7.521–7.500 (m, 1 H, Py-H), 7.44 (d, J = 7.8 Hz, 1 H, Py-H),7.16 (t, J = 6.6 Hz, 1 H, Py-H), 4.43 (s, 2 H, Py-CH_2). ^{13}C NMR (600 MHz, $CDCl_3$): 192.9, 157.6, 151.7, 149.5, 149.2, 137.2, 136.7, 127.9, 123.3, 122.1, 120.5, 35.1. Microanalysis for $C_{12}H_{10}N_2SO$ (MW = 230.29), calc. (%): C, 62.59; H, 4.38; N, 12.16. Found (%): C, 62.40; H, 5.54; N, 11.92.

Preparation of $[Fe_2(\kappa\text{-}COCH_3)(\mu\text{-}SCH_2Py)(CO)_5]$ (1). $Fe_3(CO)_{12}$ (1.09 g, 2.2 mmol) and ligand **L_1** (0.361 g, 2.2 mmol) in THF (20 mL) was heated at 70 °C for 2.5 h. The resulting reddish brown mixture was concentrated under reduced pressure and purified with column chromatography (eluent: ethyl acetate–petroleum ether = 1 : 4) to give as a red solid (0.29 g, 32%) which was crystallised from DCM/hexanes at −24 °C. IR (DCM, ν/cm^{-1}): 2046, 1986, 1969, 1919 (CO). ^{1}H NMR (400 MHz, d_6-DMSO): 8.95 (d, J = 7.9 Hz, 1 H, Py-H), 7.68 (t, J = 9.40 Hz, 1 H, Py-H), 7.38 (d, J = 9.40 Hz, 1 H, Py-H), 7.23 (t, J = 9.3 Hz, 1 H, Py-H), 4.67 (d, J = 28.8 Hz, 1 H, Py-CH_2), 4.32 (d, J = 28.8 Hz, 1 H, Py-CH_2), 1.99 (s, 3 H, FeCO–CH_3). ^{13}C NMR (600 MHz, $CDCl_3$): 219.2, 216.3, 213.3, 164.7, 155.6, 138.2, 138.2, 124.9, 124.4, 48.0, 45.0. Microanalysis for $Fe_2C_{13}H_9NSO_6$ (MW = 418.97), calc. (%): C, 37.27; H, 2.17; N, 3.34. Found (%): C, 37.65; H, 1.81; N, 3.25.

Preparation of $[Fe_2(\kappa\text{-}COCH_3)(\mu\text{-}SCH_2Py)(CO)_4PPh_3]$ (2). Complex **1** (18.70 mg, 0.045 mmol) and PPh_3 (11.71 mg, 0.09 mmol) in THF (10 mL) was heated at 55 °C for 2.5 h. The reaction mixture was evaporated to dryness under vacuum and purified with column chromatography (eluent: ethyl acetate–petroleum ether = 1 : 4) to produce a red solid (12 mg, 42%) which was recrystallised from DCM/hexanes at −24 °C. IR (DCM, ν/cm^{-1}): 1987, 1947, 1913, 1897 (CO). ^{1}H NMR (600 MHz, $CDCl_3$): 8.951 (s, 1 H, Py-H), 7.57–6.94 (m, 21 H, Ar-H and Py-H), 4.05 (s, 1 H, Py-CH_2), 3.39 (s, 1 H, Py-CH_2), 2.01 (s, 3 H, $OCCH_3$). ^{31}P NMR (600 MHz, $CDCl_3$): 46.09. Microanalysis for $Fe_2C_{30}H_{24}NSPO_5$ (MW = 653.24), calc. (%): C, 55.16; H, 3.70; N, 2.14. Found (%): C, 55.03; H, 2.96; N, 2.08.

Preparation of $[Fe_2(\kappa\text{-}Py)(\mu\text{-}SCH_2Py)(CO)_5]$ (3), $[Fe_2(\kappa\text{-}Py)'(\mu\text{-}SCH_2Py)(CO)_5]$ (4), and $[Fe_2(\kappa\text{-}Py)(\mu\text{-}SCH_2Py)(CO)_6]$ (5). $Fe_3(CO)_{12}$ (1.31 g, 2.61 mmol) and ligand **L_2** (0.60 g, 2.61 mmol) in THF (40 mL) was heated at 65 °C for 1.5 h. The reaction mixture was evaporated to dryness under vacuum and purified using column chromatography (eluent: ethyl acetate–petroleum ether = 1 : 4) to give following three products:

Complex **3** as a red solid (49.3 mg, 17%) which was recrystallised from DCM/hexanes at −24 °C. IR (DCM, ν/cm^{-1}): 2034, 1975, 1957, 1907 (CO). ^{1}H NMR (600 MHz, $CDCl_3$): 9.02 (s, 1 H, Py-H), 7.42 (d, J = 24.0 Hz, 2 H, Py-H), 7.26 (s, 1 H, Py-H), 7.15 (s, 1 H, Py-H), 6.98 (s, 1 H, Py-H), 6.78 (s, 2 H, Py-H), 6.41 (s, 1 H, Py-H), 4.47 (d, J = 15.6 Hz, 1 H, Py-CH_2), 4.05 (d, J = 15.6 Hz, 1 H, Py-CH_2). ^{13}C NMR (600 MHz, $CDCl_3$): 220.3, 216.9, 213.1, 197.0, 164.2, 154.3, 152.0, 137.7, 135.6, 131.2, 122.9, 122.1, 118.3, 44.0. Microanalysis for $Fe_2C_{16}H_{10}N_2SO_5$ (MW = 454.02), calc.: C, 42.33; H, 2.22; N, 6.17. Found: C, 41.88; H, 1.82; N, 6.16.

Complex **4** as a red solid (57 mg, 19%) which was recrystallised from DCM/hexanes at −24 °C. IR (DCM, ν/cm^{-1}): 2029, 1981, 1947, 1917 (CO). ^{1}H NMR (600 MHz, $CDCl_3$): 8.51 (s, 1 H, Py-H), 7.29 (s, 1.4 H, Py-H), 7.12 (s, 1 H, Py-H), 6.99 (s, 1 H, Py-H), 6.80 (s, 2.6 H, Py-H), 6.36 (s, 1H, Py-H), 4.44 (s, 1 H, Py-CH_2), 3.93 (s, 1 H, Py-CH_2). Anal. Calc. for $Fe_2C_{16}H_{10}N_2SO_5$ (MW = 454.02): C, 42.33; H, 2.22; N, 6.17; S, 7.06. Found: C, 41.99; H, 2.31; N, 6.12; S, 7.01.

Complex **5** as a orange-red solid (106 mg, 18%) which was crystallised from ether/hexanes at −24 °C. IR (DCM, ν/cm^{-1}): 2067, 2026, 1990, 1960 (CO). ^{1}H NMR (600 MHz, $CDCl_3$): 8.63 (s, 1 H, Py-H), 7.69 (s, 1 H, Py-H), 7.50 (s, 1 H, Py-H), 7.33 (d, J = 6.6 Hz, 1 H, Py-H), 7.22 (s, 1 H, Py-H), 7.04 (s, 2 H, Py-H), 6.64 (s, 1 H, Py-H), 3.926–3.849 (m, 2 H, Py-CH_2). ^{13}C NMR (600 MHz, $CDCl_3$): 213.6, 210.2, 191.6, 159.1, 153.6, 149.9, 137.6, 136.9, 133.3, 122.8, 122.4, 120.4, 45.5. Microanalysis for $Fe_2C_{17}H_{10}N_2SO_6$ (MW = 482.03), calc. (%):

C, 42.36; H, 2.09; N, 5.81. Found (%): C, 42.10; H, 1.69; N, 5.79.

The conversion of complexes 5 into 4

To a stirred solution of complex **5** (3.0 mg 0.006 mmol) in DCM (3.0 mL) was added trimethylamine *N*-oxide dihydrate (1.0 mg 0.013 mmol). The mixture was heated to 40 °C under stirring for 0.5 h to complete the reaction to produce a brownish red solution. IR (DCM, ν/cm^{-1}): 2029, 1981, 1947, 1917 cm^{-1} (CO).

Acknowledgements

We thank the Natural Science Foundation of China (Grant No. 20871064, 21171073), Ministry of Science and Technology of China (973 program, 2009CB220009), and the provincial government of Zhejiang for Qianjiang Professorship (X. Liu) for financial supports.

Notes and references

1 P. M. Vignais and B. Billoud, *Chem. Rev.*, 2007, **107**, 4206–4272.
2 M. Frey, *ChemBioChem*, 2002, **3**, 153–160.
3 S. Shima, O. Pilak, S. Vogt, M. Schick, M. S. Stagni, W. Meyer-Klaucke, E. Warkentin, R. K. Thauer and U. Ermler, *Science*, 2008, **321**, 572–575.
4 J. W. Peters, W. N. Lanzilotta, B. J. Lemon and L. C. Seefeldt, *Science*, 1998, **282**, 1853–1858.
5 Y. Nicolet, C. Piras, P. Legrand, C. E. Hatchikian and J. C. Fontecilla-Camps, *Structure*, 1999, **7**, 13–23.
6 S. Shima, E. J. Lyon, M. S. Sordel-Klippert, M. Kauss, J. Kahnt, R. K. Thauer, K. Steinbach, X. L. Xie, L. Verdier and C. Griesinger, *Angew. Chem., Int. Ed.*, 2004, **43**, 2547–2551.
7 S. Shima and R. K. Thauer, *Chem. Rec.*, 2007, **7**, 37–46.
8 T. Hiromoto, K. Ataka, O. Pilak, S. Vogt, M. S. Stagni, W. Meyer-Klaucke, E. Warkentin, R. K. Thauer, S. Shima and U. Ermler, *FEBS Lett.*, 2009, **583**, 585–590.
9 T. Hiromoto, E. Warkentin, J. Moll, U. Ermler and S. Shima, *Angew. Chem., Int. Ed.*, 2009, **48**, 6457–6460.
10 S. Shima and U. Ermler, *Eur. J. Inorg. Chem.*, 2011, 963–972.
11 S. Shima, M. Schick and H. Tamura, in *Methods in Enzymology: Methods in Methane Metabolism, Pt A*, ed. A. C. Rosenzweig and S. W. Ragsdale, 2011, vol. 494, pp. 119–137.
12 S. Shima, M. Schick, J. Kahnt, K. Ataka, K. Steinbach and U. Linne, *Dalton Trans.*, 2012, **41**, 767–771.
13 X. F. Wang, Z. M. Li, X. R. Zeng, Q. Y. Luo, D. J. Evans, C. J. Pickett and X. M. Liu, *Chem. Commun.*, 2008, 3555–3557.
14 S. Shima, E. J. Lyon, R. K. Thauer, B. Mienert and E. Bill, *J. Am. Chem. Soc.*, 2005, **127**, 10430–10435.
15 Y. S. Guo, H. X. Wang, Y. M. Xiao, S. Vogt, R. K. Thauer, S. Shima, P. I. Volkers, T. B. Rauchfuss, V. Pelmenschikov, D. A. Case, E. E. Alp, W. Sturhahn, Y. Yoda and S. P. Cramer, *Inorg. Chem.*, 2008, **47**, 3969–3977.
16 B. Li, T. Liu, C. V. Popescu, A. Bilko and M. Y. Darensbourg, *Inorg. Chem.*, 2009, **48**, 11283–11289.
17 M. Salomone-Stagni, F. Stellato, C. M. Whaley, S. Vogt, S. Morante, S. Shima, T. B. Rauchfuss and W. Meyer-Klaucke, *Dalton Trans.*, 2010, **39**, 3057–3064.
18 B. V. Obrist, D. F. Chen, A. Ahrens, V. Schunemann, R. Scopelliti and X. L. Hu, *Inorg. Chem.*, 2009, **48**, 3514–3516.
19 A. M. Royer, T. B. Rauchfuss and D. L. Gray, *Organometallics*, 2009, **28**, 3618–3620.
20 D. F. Chen, R. Scopelliti and X. L. Hu, *J. Am. Chem. Soc.*, 2010, **132**, 928–929.
21 D. F. Chen, R. Scopelliti and X. L. Hu, *Angew. Chem., Int. Ed.*, 2010, **49**, 7512–7515.
22 A. M. Royer, M. Salomone-Stagni, T. B. Rauchfuss and W. Meyer-Klaucke, *J. Am. Chem. Soc.*, 2010, **132**, 16997–17003.
23 P. J. Turrell, J. A. Wright, J. N. T. Peck, V. S. Oganesyan and C. J. Pickett, *Angew. Chem., Int. Ed.*, 2010, **49**, 7508–7511.
24 J. A. Wright, P. J. Turrell and C. J. Pickett, *Organometallics*, 2010, **29**, 6146–6156.
25 D. Chen, R. Scopelliti and X. Hu, *Angew. Chem., Int. Ed.*, 2011, **50**, 5671–5673.
26 D. F. Chen, A. Ahrens-Botzong, V. Schuemann, R. Scopelliti and X. L. Hu, *Inorg. Chem.*, 2011, **50**, 5249–5257.
27 D. F. Chen, R. Scopelliti and X. L. Hu, *Angew. Chem., Int. Ed.*, 2011, **50**, 5670–5672.
28 M. J. Corr and J. A. Murphy, *Chem. Soc. Rev.*, 2011, **40**, 2279–2292.
29 D. Seyferth, G. B. Womack, C. M. Archer and J. C. Dewan, *Organometallics*, 1989, **8**, 430–442.
30 D. Seyferth, G. B. Womack and J. C. Dewan, *Organometallics*, 1985, **4**, 398–400.
31 X. F. Wang, Z. M. Li, F. Peng, X. Ru, X. R. Zeng, Q. Y. Luo and X. M. Liu, *Inorg. Chim. Acta*, 2009, **362**, 2065–2067.
32 G.-J. M. Gruter, O. S. Akkerman and F. Bickelhaupt, *J. Org. Chem.*, 1994, **59**, 4473–4481.
33 J. A. Drewry, S. Fletcher, H. Hassan and P. T. Gunning, *Org. Biomol. Chem.*, 2009, **7**, 5074–5077.
34 R. Fornasier, P. Scrimin, P. Tecilla and U. Tonellato, *J. Am. Chem. Soc.*, 1989, **111**, 224–229.
35 M. B. Skaddan and J. A. Katzenellenbogen, *Bioconjugate Chem.*, 1998, **10**, 119–129.
36 K. J. C. van Bommel, M. R. de Jong, G. A. Metselaar, W. Verboom, J. Huskens, R. Hulst, H. Kooijman, A. L. Spek and D. N. Reinhoudt, *Chem.–Eur. J.*, 2001, **7**, 3603–3615.
37 D. J. Evans and C. J. Pickett, *Chem. Soc. Rev.*, 2003, **32**, 268–275.
38 X. M. Liu, S. K. Ibrahim, C. Tard and C. J. Pickett, *Coord. Chem. Rev.*, 2005, **249**, 1641–1652.
39 F. F. Xu, C. Tard, X. F. Wang, S. K. Ibrahim, D. L. Hughes, W. Zhong, X. R. Zeng, Q. Y. Luo, X. M. Liu and C. J. Pickett, *Chem. Commun.*, 2008, 606–608.
40 Y. W. Wang, Z. M. Li, X. H. Zeng, X. F. Wang, C. X. Zhan, Y. Q. Liu, X. R. Zeng, Q. Y. Luo and X. M. Liu, *New J. Chem.*, 2009, **33**, 1780–1789.
41 W. Zhong, Y. Tang, G. Zampella, X. F. Wang, X. L. Yang, B. Hu, J. A. Wang, Z. Y. Xiao, Z. H. Wei, H. W. Chen, L. De Gioia and X. M. Liu, *Inorg. Chem. Commun.*, 2010, **13**, 1089–1092.
42 Y. F. Yu, J. Gallucci and A. Wojcicki, *J. Am. Chem. Soc.*, 1983, **105**, 4826–4828.
43 J. B. Hoke, J. C. Dewan and D. Seyferth, *Organometallics*, 1987, **6**, 1816–1819.
44 Z. Y. Xiao, Z. H. Wei, L. Long, Y. L. Wang, D. J. Evans and X. M. Liu, *Dalton Trans.*, 2011, **40**, 4291–4299.
45 Y. Tang, Z. Wei, W. Zhong and X. Liu, *Eur. J. Inorg. Chem.*, 2011, **2011**, 1112–1120.
46 C. C. Yin and A. J. Deeming, *J. Chem. Soc., Dalton Trans.*, 1975, 2091–2096.
47 K. Godula, B. Sezen and D. Sames, *J. Am. Chem. Soc.*, 2005, **127**, 3648–3649.
48 P. Das, M. Borah, F. Michaud, F. Y. Pétillon and P. Schollhammer, *Inorg. Chim. Acta*, 2011, **376**, 641–644.
49 C. Tard and C. J. Pickett, *Chem. Rev.*, 2009, **109**, 2245–2274.
50 M. Bruschi, G. Zampella, P. Fantucci and L. De Gioia, *Coord. Chem. Rev.*, 2005, **249**, 1620–1640.
51 G. Zampella, C. Greco, P. Fantucci and L. De Gioia, *Inorg. Chem.*, 2006, **45**, 4109–4118.
52 L. Bertini, M. Bruschi, L. de Gioia, P. Fantucci, C. Greco and G. Zampella, in *Atomistic Approaches in Modern Biology: From Quantum Chemistry to Molecular Simulations*, ed. M. Reiher, Springer-Verlag, Berlin, Heidelberg, 2007, vol. 268, pp. 1–46.
53 G. Zampella, P. Fantucci and L. De Gioia, *J. Am. Chem. Soc.*, 2009, **131**, 10909–10917.
54 P.-Y. Orain, J.-F. Capon, F. Gloaguen, F. Y. Petillon, P. Schollhammer, J. Talarmin, G. Zampella, L. De Gioia and T. Roisnel, *Inorg. Chem.*, 2010, **49**, 5003–5008.
55 Z. Xiao, F. Xu, L. Long, Y. Liu, G. Zampella, L. De Gioia, X. Zeng, Q. Luo and X. Liu, *J. Organomet. Chem.*, 2010, **695**, 721–729.
56 G. Zampella, P. Fantucci and L. De Gioia, *Chem. Commun.*, 2010, **46**, 8824–8826.

57 M. T. Olsen, D. L. Gray, T. B. Rauchfuss, L. D. Gioia and G. Zampella, *Chem. Commun.*, 2011, **47**, 6554–6556.
58 H. Wang, Y. Xie, R. B. King and H. F. Schaefer, *J. Am. Chem. Soc.*, 2006, **128**, 11376–11384.
59 R. Ahlrichs, M. Bar, M. Haser, H. Horn and C. Kolmel, *Chem. Phys. Lett.*, 1989, **162**, 165–169.
60 J. P. Perdew, *Phys. Rev. B*, 1986, **33**, 8822–8824.
61 A. D. Becke, *Phys. Rev. A: At., Mol., Opt. Phys.*, 1988, **38**, 3098–3100.
62 J. N. Harvey and M. Aschi, *Faraday Discuss.*, 2003, **124**, 129–143.
63 J. L. Carreon-Macedo and J. N. Harvey, *Phys. Chem. Chem. Phys.*, 2006, **8**, 93–100.
64 L. Bertini, M. Bruschi, L. De Gioia and P. Fantucci, *J. Phys. Chem. A*, 2007, **111**, 12152–12162.

